# Front End Electronics for Neutron- Gamma Spectrometer Device

by

Kush Gupta

A Thesis Presented in Partial Fulfillment
of the Requirements for the Degree
Master of Science

Approved April 2017 by the
Graduate Supervisory Committee:

Hugh Barnaby, Chair
Craig Hardgrove
Sule Ozev

ARIZONA STATE UNIVERSITY

May 2017

ABSTRACT

With the natural resources of earth depleting very fast, the natural resources of other celestial bodies are considered a potential replacement. Thus, there has been rise of space missions constantly and with it the need of more sophisticated spectrometer devices has increased. The most important requirement in such an application is low area and power consumption.

To save area, some scintillators have been developed that can resolve both neutrons and gamma events rather than traditional scintillators which can do only one of these and thus, the spacecraft needs two such devices. But with this development, the requirements out of the readout electronics has also increased which now need to discriminate between neutron and gamma events.

This work presents a novel architecture for discriminating such events and compares the results with another approach developed by a partner company. The results show excellent potential in this approach for the neutron-gamma discrimination and the team at ASU is going to expand on this design and build up a working prototype for the complete spectrometer device.

ACKNOWLEDGMENTS

I would like to take this opportunity and thank my advisor Dr. Hugh Barnaby for all the effort he has done towards this project and my academic development. It was a great learning opportunity to be a part of his research team. I am also thankful to Dr. Hardgrove for giving us the opportunity to work on this project and Dr. Ozev for being on my thesis committee. I also want to thank the excellent faculty at ASU who I encountered.

I would also like to thank my colleagues and friends in Qiantong, Sanchit, Bingbing, Shiqing, Miao, Mohan, Shrikant, Tushar, Blayne, Soroush and countless other people I met at ASU for being a constant source of motivation and giving me the opportunity to grow with them.

Finally, I would like to thank the team at Alphacore for giving me the opportunity to apply my technical skills in a challenging work environment.

TABLE OF CONTENTS

Page

CHAPTER Page

# LIST OF TABLES

Table Page

LIST OF FIGURES

Figure Page

# CHAPTER 1

# Introduction

## 1.1 Purpose of this work

Even though man has explored the Moon and Mars, it remains a mystery whether we are alone in the Universe. This curiosity has led to the large number of space missions (for even more reasons check [1]). In these missions, scientists and engineers have employed key strategies to see what cannot be seen by the eye, which is analyzing the material composition of the surface of a planetary object.

Since water is essential for life, its existence on a planetary object would suggest a certain probability of life there [2]. Thus, to support the search for life, a way to accurately determine the presence of water is almost essential.

Other than searching for water, a space mission is also useful in exploring the natural resources of a planetary body, and especially those which are very scarce on Earth and hence expensive. This is for the future possibility of missions that conduct mineral excavations. The natural resources found on a body are determined by the first estimating abundance of various elements and then doing empirical analysis to find the chemical composition of the surface [3], [4], [5], [6].

The objective of this thesis is to describe the development of a single scintillator neutron gamma ray spectrometer device(SINGR) that can be used for water and other material identification on remote space missions. Neutrons are interatomic particles unlike gamma rays which are electromagnetic waves. Due to their de Broglie wavelength, neutrons are

also a source of radiative energy and can be used as electromagnetic waves for spectroscopy. As discussed in section 1.2, we need both gamma ray spectroscopy and neutron spectroscopy for extracting the elemental composition and Hydrogen content. Detecting gamma rays and neutrons typically require two separate detection devices which takes a big portion out of the limited space on a CUBESAT. With a single detector crystal, there are challenges related with the discrimination of gamma rays and neutrons because both of these provide different information about the composition of a surface and as such it is imperative to know whether a pulse is gamma- ray or neutron. So, in addition to measuring the energy of a signal, we have an additional challenge of discriminating gamma- rays and neutrons.

We need to identify three important characteristics about incident pulses to determine whether it is a neutron or a gamma ray. We must detect the pulse width, energy to the best resolution (which is the most important measurement in a spectrometer) and also the event rate such that we can construct a probability distribution function with time. The need of monitoring the event rate with time has been established in Section 1.2. [7] gives a brief overview of the instruments on Curiosity rover.

### 1.2 Overview of application

Now that it is established that we need both abundances of various elements and water for the characterization of a surface in a space mission. This section deals with how this information is acquired using a neutron and gamma ray detector.

The absorption of neutrons might result in the atoms going to unstable state and resulting in gammas emitted on nuclear fission. Or the neutron may collide with lighter nucleus (low atomic number) and lose energy. Thus, we get a large number of neutrons and gamma-rays distributed over a period of time. These particles or electromagnetic waves, in the case of gamma-rays, have a varied range of energies and different probability distribution that are representative of the material under consideration.

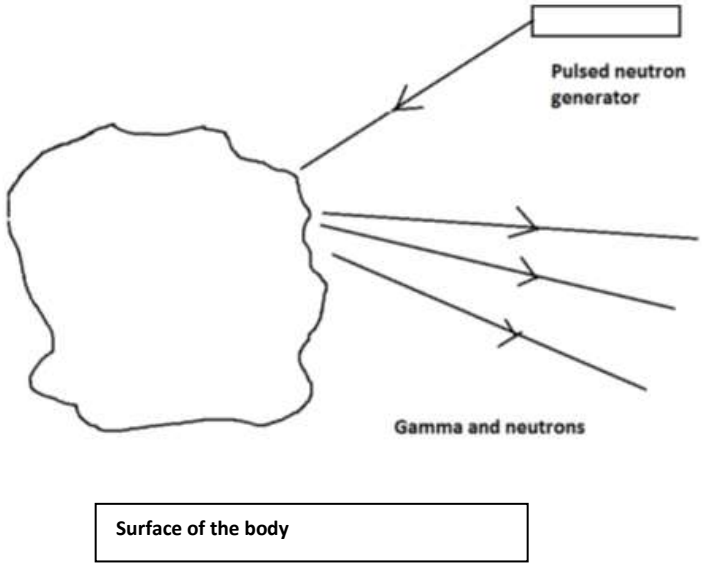


Figure 1.1: A schematic diagram of the surface exposed to neutron source

### 1.2.1 Gamma-ray spectroscopy

When we stimulate the material with pulsed neutron generator, gamma -rays are emitted during the decay of the excited atom or nucleus. The energy of these gamma-rays is a function of the material that was illuminated by the neutron source. This is a basic principle of nuclear spectroscopy. [8] discusses the basic principles while [9] lists a variety of

methods for gamma spectroscopy. If we measure the energy of these gamma-rays, we can determine the material's constituent elements. In addition to the presence of an element, we also need to measure the abundance of the element so that we can do stoichiometric analysis [10] and to subsequently constrain the composition of the materials near the detector. For this we need to monitor how many of these events happen. So, we need to measure the energy of the gamma-rays and the rate of the events.

### 1.2.2 Neutron spectroscopy

Neutrons are neutral particles. They cannot interact with the electrons in an atom and go straight to the bulk of the atom or the nucleus. When a neutron collides a nucleus, it transfers a significant part of its energy to the colliding nucleus with the energy transferred being a function of the atomic number [11],[12]. So, if the material under test is composed of lighter elements, the energy transferred will be considerably higher than heavier elements. Thus, hydrogen shows the highest amount of neutron scattering [13]. Oxygen and carbon are also visible in neutron scattering spectrum. Thus, neutron spectroscopy is a very good measure of water (as water is $H_2O$).

We illuminate the surface with fast neutrons and then detect the energy of the neutrons received from the surface. A large decrease in the energy of the neutrons indicates the presence of hydrogen.

The expected distribution of neutrons in time observed by a spectrometer for a surface rich in hydrogen when excited by the pulsed neutron source is like follows.

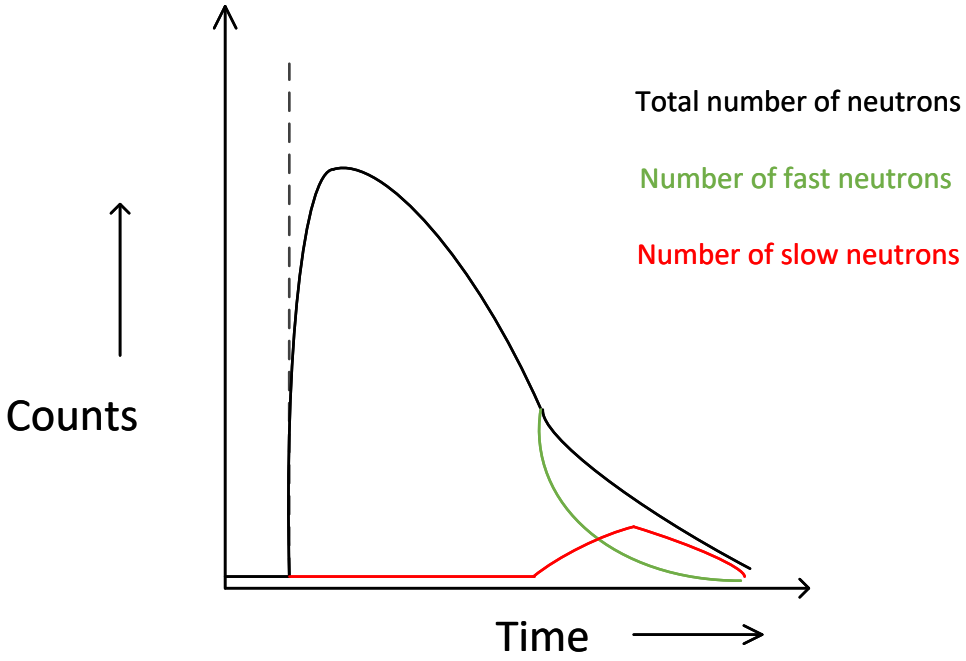


Figure 1.2: Relative neutron count rate

Initially the number of observed neutrons increases exponentially. This corresponds to the neutron source turned on. As it is turned off, the neutrons start to disperse away and thus the number of neutrons observed decreases gradually. The second curve represents the fast neutrons which follows the first curve for some time and then start decreasing faster. This is because a lot of neutrons lose energy because of neutron scattering. These neutrons then show in the slow neutron curve marked in red. Notice the straight line on either side that depicts the background neutrons.

We want to measure the energy of the neutrons so that we can classify them in slow neutrons and fast neutrons. Further, we want to monitor the rate of such events.

Finally, as already discussed, there is the need of discrimination of the neutron and gamma-ray which arises because the innovative crystal used in this project.

### 1.3 Outline

Chapter-2 in this document expands on the various components of the system we are developing which includes the detector in addition to the electronics. The basic of the physics of operation has also been expanded in this chapter.

Chapter-3 presents the design and the results are summarized in Chapter-4. Finally the work is concluded in Chapter-5.

# CHAPTER 2

## System Description

The basic structure of the spectrometer system is as shown below.

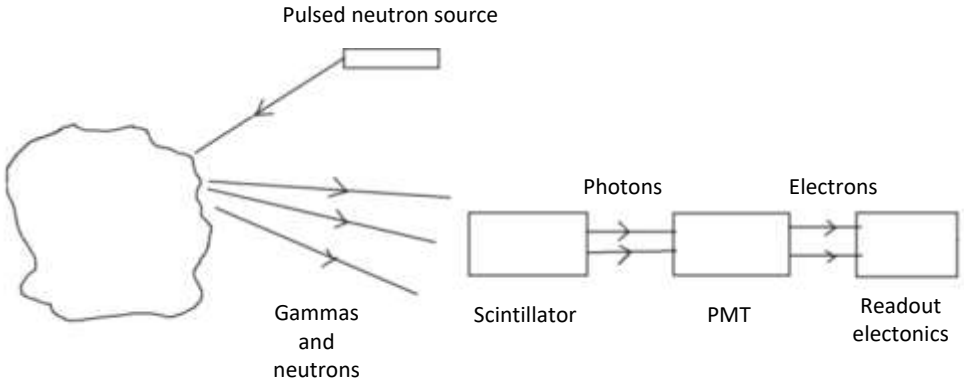


Figure 2.1: Schematic diagram of the spectrometer device

This chapter will discuss the three basic components in detail, i.e., the scintillator, the photomultiplier tube (PMT), and, most importantly, the readout electronics.

### 2.1 Scintillator

The scintillator or detector is the part of the receiver closest to the return radiation signal, as shown in Fig. 2.1. Scintillator is a material which creates photons when excited by radiation. [14] discusses the major classes of scintillators and current trends. This definition makes sense for a neutron but a gamma-ray is already an electromagnetic wave and as such it is already a photon. Then why do we even need to convert the gamma-ray to a photon? This is because gamma-rays are on the extreme end of EM wave spectrum and as such they have a very high frequency. Most of the photosensitive materials are not sensitive to gamma-rays directly. In fact, gamma-ray interactions with matter are very limited due to

their high energy. For spectroscopy, we still need to detect radiation over a wide range of energies. So, we first need to consider how photon interaction with matter depends on energy.

### 2.1.1 Interactions of gamma-ray with matter

Of all the ways photons interact with matter [15], only the following three are important in relevance to spectroscopy:

A) Photoelectric effect:

The photoelectric effect is the emission of electrons from a material in response to light. Photons of low energy show photoelectric effect.

The photoelectric effect is the cleanest way to detect a photon because it is completely lost in this process and transfers its energy to an electron less the work function of the electron (the energy that binds the electron to its atom)

Mathematically, $KE = h\upsilon + E_0$ where $h\upsilon$ is the energy of the incident photon, $\upsilon$ being the frequency of this photon, h is Planck's constant and $E_0$ is the work function of the material. This is the classical definition of photoelectrical effect ,for a more accurate treatment, refer to [16].

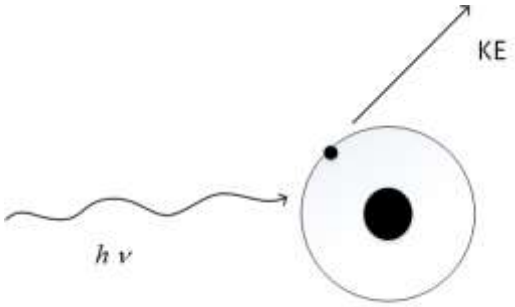


Figure 2.2: Representation of photoelectric effect

This electron might lead to secondary emissions but then it will emit new electrons such that the sum of kinetic energies of all these electrons is still equal to the energy of the incident photon minus the work function.

B) Compton scattering:

Compton scattering is similar to diffraction but on a microscopic scale. The compton effect is shown by mid to higher energy photons like gamma-rays when they have higher energies than that required for photoelectric effect.

When this photon collides with a material, it is scattered, meaning that changes the direction of the photon by an angle ɵ as it absorbs energy. It also results in the emission of the electron with a kinetic energy equal to the difference of energy of the incident, and scattered photon minus the binding energy of the electron. The electron again follows a path with an angle of ɵ to the original direction of the radiation but on the other side. This is as shown below:

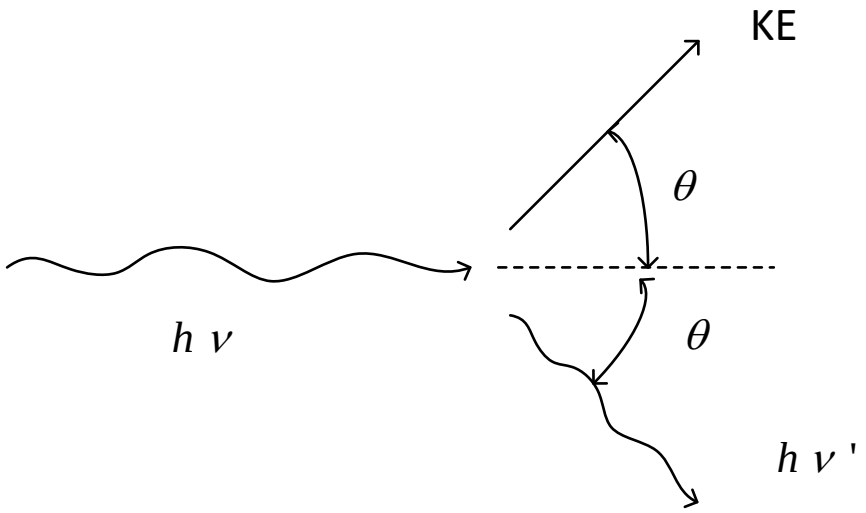


Figure 2.3: Representation of Compton scattering

The energy of these two emitted particles is dependent on this grazing angle ɵ and in normal circumstances a wide distribution of these energies is observed. [17] and [18] present a more detailed mathematical treatment of Compton Effect.

The resulting photons might generate further photoelectrons or lead to another instance of Compton scattering. So, this higher energy radiation will lead to a higher number of photoelectrons.

C) Pair production

In pair production, the highest energy photon (it may also be a gamma ray) interacts with the nucleus of the atom and generates a positron and electron pair. Thus, the incident photon must have energy greater than the binding energy of two electrons (positron also has the same charge and mass). This total binding energy is equal to 1.02MeV[19]. Any excess energy of the photon is shared equally between the electron and the positron. The positron is not a stable particle and it finally combines with an electron and generates two gamma-rays each with half the binding energy. Then these can lead to further photoelectric or Compton effects. [20] discusses the mathematics of pair production while [21] discusses pair production in a different light, to measure structural properties of a material by using high energy gammas to generate positrons and then observing their lifetime.

Thus, high energy gamma-rays can interact with the scintillator to generate photoelectrons or other photon with reduced energies. The low energy photons can

then go to the photomultiplier tube (PMT), see Figure 2.1, and then generate photoelectrons and the photoelectrons already generated in the scintillator are multiplied even further. The PMT multiplies the number of photoelectrons by secondary emissions. Photoelectrons with higher kinetic energies have a higher yield, but there is an upper bound since the very high energy secondary electrons not being able to escape the PMT.

Thus, the scintillator converts the gamma rays into photoelectrons and lower energy photons.

### 2.1.2 Detection of neutrons

Neutrons are detected by absorptive reactions. Typically, in a scintillator, Li and $Cs^{3+}$ are used to detect the neutrons. Li can absorb a neutron and will generate an alpha particle and a triton, both having kinetic energies depending on the energy of the incident neutron. These particles transfer energy to $Cs^{3+}$ and emit photons. A single neutron can generate a burst of photons. [22] discusses various classes of neutron spectroscopy and their principles. The reaction used in the scintillator(CLYC) used in this particular thesis releases fixed energy photon (3.2MeV) independent of the energy of the incident neutron[23].

Thus, it is not possible to detect neutron energy. In order to separate the slow neutrons events from fast neutron events, the detector will use two scintillator tubes. One of these tubes will be physically shielded from the environment such that only neutrons with energy higher than a threshold can reach the detector. Thus, we will get two different probability

functions from the two tubes, one with only fast neutrons, the other with both fast and slow neutrons. Thus, we can estimate the rate of slow neutrons events from this as well.

### 2.1.3 Scintillator properties

The material used for scintillator in this work is $Cs_2YLiCl_6$:Ce or CLYC. CLYC was developed by Radiation Monitoring Devices (RMD) Inc. RMD has been closely working with the team at ASU in developing this spectrometer device. The scintillation properties of CLYC, the scintillator used in this work has been widely studied for its properties and pulse shape discrimination as discussed in [24], [25], [26], [27], [28], [29], [30] and [31].

Of all the elements present in CLYC, Li and Ce are used to detect the neutrons while the rest of the elements are sensitive to the gamma-rays. So, the most important feature of this material is that it can detect both the neutron counts and the gamma ray spectrum.

CLYC has a different pulse shape for gamma-rays than neutrons. This can be distinguished by looking at the decay of the pulses detected for gamma-ray and neutrons.

A sample neutron pulse as compared to gamma is shown below:

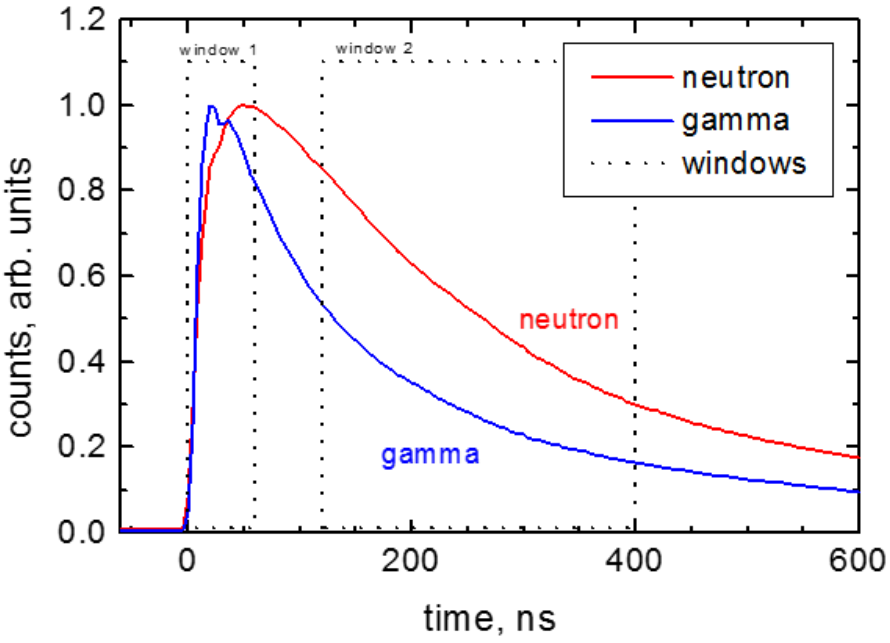


Figure 2.4: Neutron pulse V/S Gamma pulse as detected by CLYC

CLYC also has a high detection efficiency (meaning that number of neutrons actually detected is very high) for neutron and very good energy resolution for gamma ray spectroscopy (3.9% FWHM at 662KeV). Energy resolution is a measure of the monochromaticity of the detector. No detector is perfect. So, if we were to use a detector on a perfectly monochromatic source, it will still produce a spectrum with variation equal to the energy resolution. Energy resolution is measured as a width of the spectrum (FWHM) as a percentage of the energy.

## 2.2 Photomultiplier tube

As the name suggests the photomultiplier tube is used to multiply the number of photons received. These tubes can multiply the detected current a million times. A conventional photomultiplier tube is shown below:

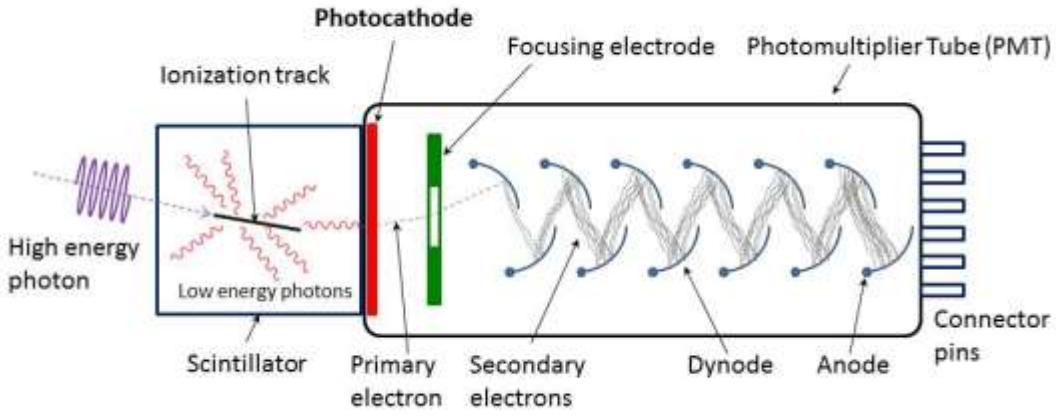


Figure 2.5: Schematic diagram of a PMT [32]

Figure 2.5 shows a conventional PMT used in gamma ray spectroscopy. As shown in the figure, the PMT has a photocathode on one end and then a series of dynodes to multiply the current. These dynodes are progressively connected to a higher voltage.

The photocathode converts photons to photoelectrons. The primary photoelectrons or the photoelectrons at the photocathode are attracted to the positive dynode and get accelerated. This accelerated electron hit the dynode and lead to secondary emission. The number of electrons emitted from this secondary emission is a function of the energy of the primary photoelectrons. Thus, photon with higher energies which produce photoelectrons with higher kinetic energy get multiplied to a larger number of photoelectrons. These photoelectrons are converted to photocurrent and sent onto the subsequent circuit.

Photocurrent is the charge of electron multiplied by the number of electrons crossing an imaginary cross section along the conductor. Thus, the energy of incident gamma ray (on the scintillator) is equal to the total energy of the current pulse generated. Note that even though it is a single gamma ray particle it will lead to a current pulse because of the way the detection and photo-multiplication works. There will be a large number of photoelectrons getting multiplied eventually and they will have different sources (one might be generated from an electron generate one dynode away while the other might be an electron generated several dynodes before). Thus, it will generate a complete pulse instead of an abrupt Dirac-function like distribution.

For this project, we are using Hamamatsu R11265 for the photomultiplier tube with a power supply of 800V. R11265 is a 12-stage, head-on type photomultiplier tube [33], [34]. For a supply of 800V, it offers a gain of $3*10^5$. For the power supply we are using Ortec-555H which generates 800V from a different 5V supply. For more details about operation and properties of Photomultiplier Tube, refer to [35]

### 2.3 Readout Electronics

After the PMT, we have the readout electronics. All of the system used before this stage has been developed or recommended by RMD Inc. In fact, RMD has already developed a complete system including the readout as well. The problem with their approach is that they are using FPGAs for data processing which have a very high power consumption. So, main challenge is to bring the power consumption down. The plan is to do the signal

processing with basic analog and digital components such that there is no need to use power hungry FPGAs. This is not conducive for low power satellites, like CUBESATS.

The purpose of the readout is to perform analog and digital processing of the information available and convert it into a more useful form. Ideally we want to convert this information into digital bits that can be directly loaded into the satellites main computer. This flow of information in the full system is summarized in the following figure.

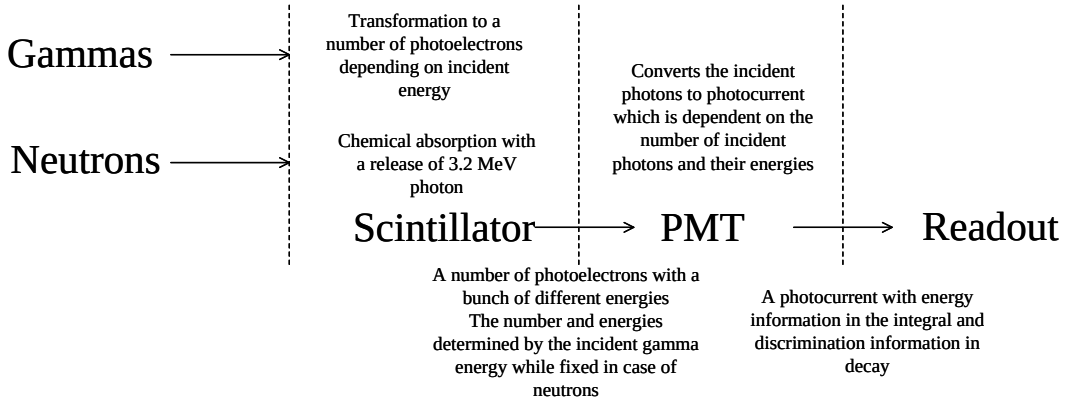


Figure 2.6: Energy transformation in the system

Up to the readout, the system has created a photocurrent with a decay time signifying whether it is a neutron or gamma and a total charge (i.e., the integral of the current pulse) which determines the energy of the incident particle. A voltage and a current source are interchangeable by the principles of Thevenin's theorem and Norton's theorem so the photocurrent can be modelled using a voltage source with a series resister for the next section. This is because using a voltage source makes the analysis much more intuitive rather than a current source. Developing the readout electronics is the main focus of the work done on this thesis. Chapter-3 covers the design of the readout electronics in detail.

# CHAPTER 3

## Design

### 3.1 Interfacing with PMT

We need to discriminate gamma and neutrons but first we need to correctly interface with the signal to consider loading and match properly. Without this, we will not be able observe any signal in the rest of the circuit.

We modelled the input signal with a voltage source and a series resistance. After thorough testing, it was determined that the Thevenin resistance out of the PMT was 300KΩ. We therefore modelled the PMT output as a piecewise linear voltage source with a series resistance of 300kΩ. This piecewise linear signal is reconstructed from real data collected from the CLYC.

In order to match the output resistance, a "buffer" stage was designed as shown in Fig. 3.1

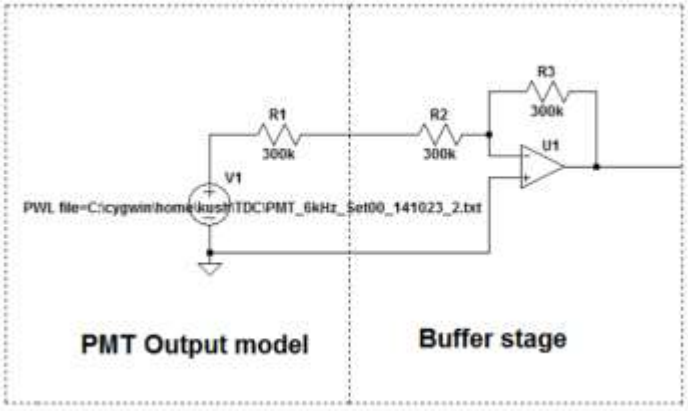


Figure 3.1: Interface with PMT

### 3.2 Extracting timing information from variable decay

The following figure shows an average neutron pulse against an average gamma ray pulse.

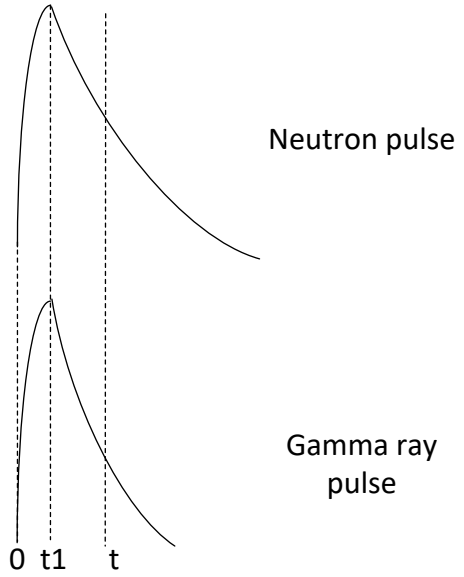


Figure 3.2: A neutron pulse compared to a gamma ray pulse

As the figure shows, the neutron dies way slower than the gamma ray pulse. So, we can use the slower decay of the neutron as its defining characteristic.

The principle of this design is that the time at which the pulse falls to A/2 respective to the time of start of this pulse is directly proportional to the rate of decay of the pulse and independent of the amplitude.

This is proved as follows:

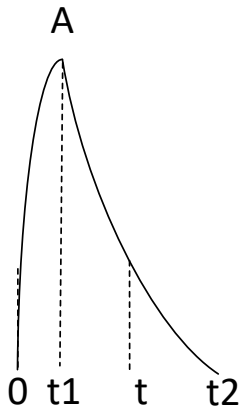


Figure 3.3: A sample pulse representing the dimensions

As shown in Figure 3.3, the pulse can be broken in two parts: from 0 to t1 and t1 to t2.

Note that the time at which the pulse starts is considered 0 as we are calculating all times with reference to the start of the pulse.

From 0 to t1, the pulse can be approximately represented as an exponential function of the form $A(1 - e^{\frac{-t}{\tau}})$

Now it will peak at t1 with the value $A(1 - e^{\frac{-t1}{\tau}})$ we denote as p0.

From t1 to t2, the pulse can be represented as another exponential function of the form $[A(1 - e^{\frac{-t1}{\tau}})]\ (\ e^{\frac{-t}{\tau 1}})$

So, pulse p(t) = $\begin{cases} A(1 - e^{\frac{-t}{\tau}}) & , \quad 0 \leq t \leq t1 \\ [A(1 - e^{\frac{-t1}{\tau}})]\ (\ e^{\frac{-(t-t1)}{\tau 1}}), & t1 \leq t \leq t2 \end{cases}$

Now a gamma is different than a neutron in the rate of decay which is represented by the variable τ1. For a fixed t, t-t1 is fixed and the exponent of e is dependent on τ1. If τ1 is

higher, the exponent will be smaller and the rate of decay will be lower. If $\tau 1$ is lower, rate of decay will be higher.

Thus, a neutron will have a higher $\tau 1$ than a gamma ray.

Now, we want to find time t when p(t)=p0/2

Thus, $p0( e^{\frac{-(t-t1)}{\tau 1}}) = \frac{p0}{2}$

Or $e^{\frac{-(t-t1)}{\tau 1}}) = \frac{1}{2}$

Taking natural log on both sides:

Thus, $\frac{(t-t1)}{\tau 1}$ = Ln 2

Or t = t1+ $\tau 1$ Ln2

As we can see, t is dependent on only the time of peak t1 and decay constant t1, not on the pulse amplitude, which is what we want.

**Dependence on t1:**

As we discussed in the last section, the time at which the pulse become half is dependent on the time of occurrence of peak. However, this peak is a function of the incident energy. So, for an equal incident energy, the time t1 is the same both for neutron and gamma ray. It is also assumed to be small so we can say

Thus, t ≈ $\tau$1 Ln2

The architecture proposed follows a basic model shown below:

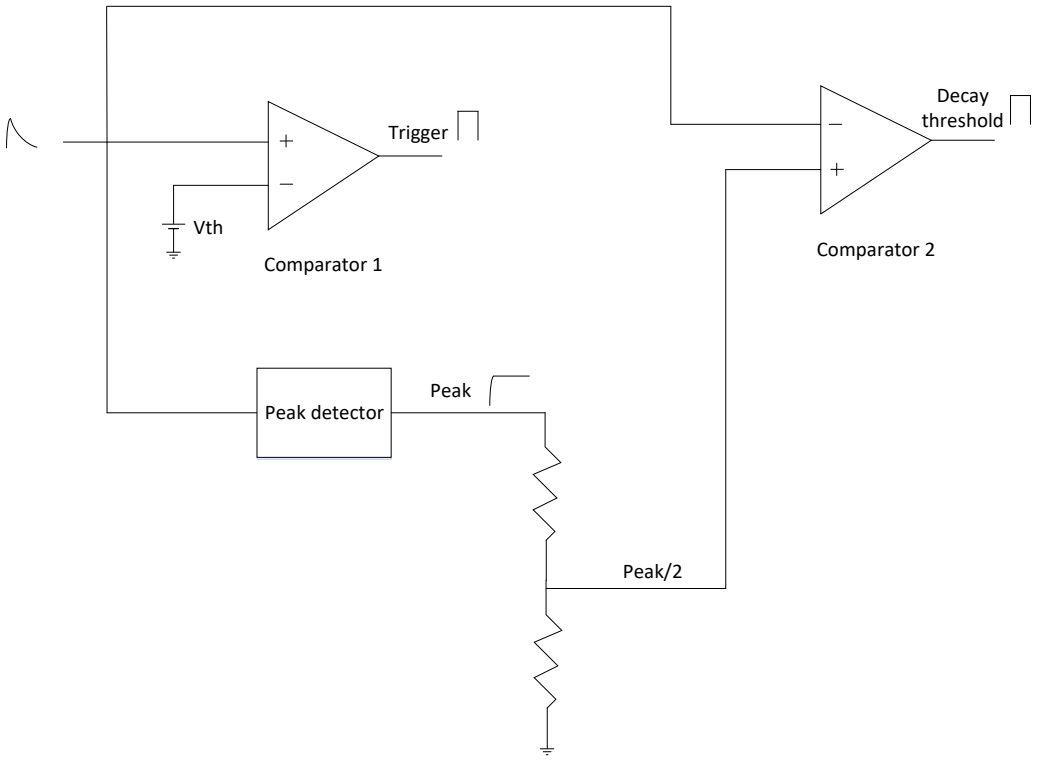


Figure 3.4: A basic model of the architecture

The schematic diagram for the full analog front end for pulse width and energy discrimination is shown below:

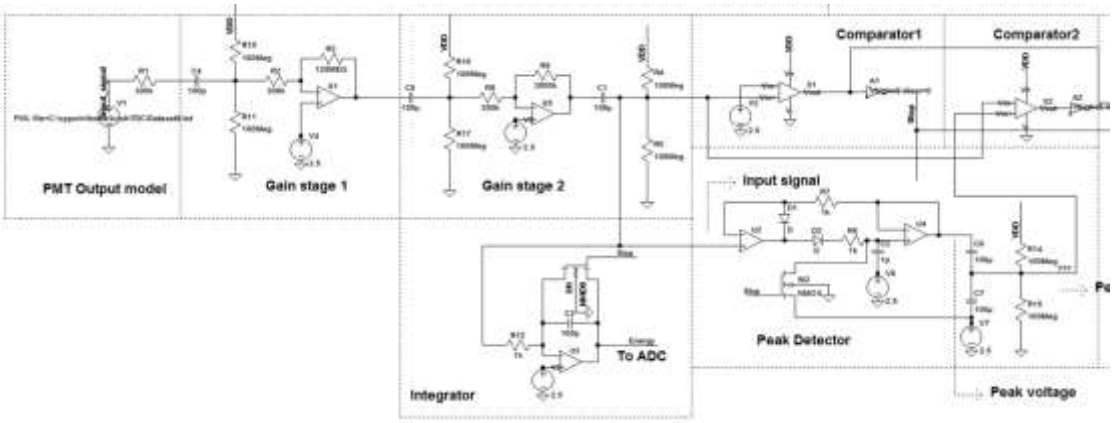


Figure 3.5: Schematic diagram of the circuit

Here the "buffer" stage is used to provide some gain as well. It is followed by another amplifier gain stage to increase the gain and make it non- inverting before the comparator.

These opamps need to have a gain bandwidth of the order of 2GHz in order to preserve the fast response of gamma. But such opamps are readily available [36].

AC coupling is used before and after both the gain stages so that we maximize dynamic range and control the impact of offset voltages.

To reduce the effect of noise on the timing signals hysteresis comparators are used. $V_{thl}$ is 10mV and $V_{thh}$ is 20mV. If we do not use a hysteresis comparator, the output of the comparator can switch between low and high several times because of thermal noise if the transition region between high and low is not very steep. A hysteresis comparator prevents this because it provides a cushion equal to the hysteresis voltage between low to high and high to low transition. Most of the commercial comparators have a hysteresis programmed into it but some vendors also provide application notes for adding external Hysteresis so it can be user defined, one such example is [37].

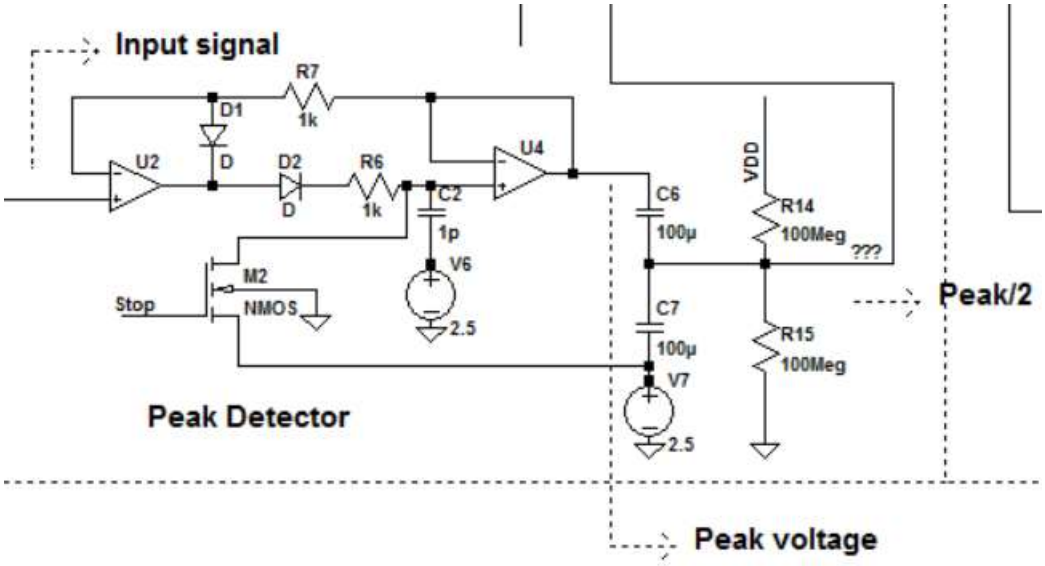


Figure 3.6: Zoomed in version of the peak detector

An OPAMP based peak detector is used for detecting Peak and Peak/2.

When the input voltage is increasing, the non-inverting terminal of the OPAMP U2 is higher than the inverting terminal so the output voltage of U2 is higher than what is already deposited on the capacitor C2. This make the diode D2 forward biased and charges to the capacitor C2 to this new value. The inverting input of the OPAMP U4 is driven to the same voltage as the non-inverting input by the unity gain feedback. This results in a finite current through resister R7 which changes the inverting input to the same value as the non-inverting input.

Now when the voltage start decreasing again, the output voltage of OPAMP U2 is negative while the voltage on the capacitor C2 is equal to the peak voltage. At this point, the diode D1 becomes forward biased and keeps the charge stored on the capacitor C2 as it is. For a more detailed explanation on peak detectors, refer to [38]

After this peak detector, we have used a capacitor divider to get the Peak/2. A capacitor divider is used in place of a resister divider because it serves the dual purpose of blocking DC and getting voltage divided by 2. Then again two resisters are used to set the DC level back to VDD/2.

### 3.3 Differentiating gamma and neutron from the timing information

As shown in section 3.3, we get the timing information out of the signal received from PMT. This is shown as below:

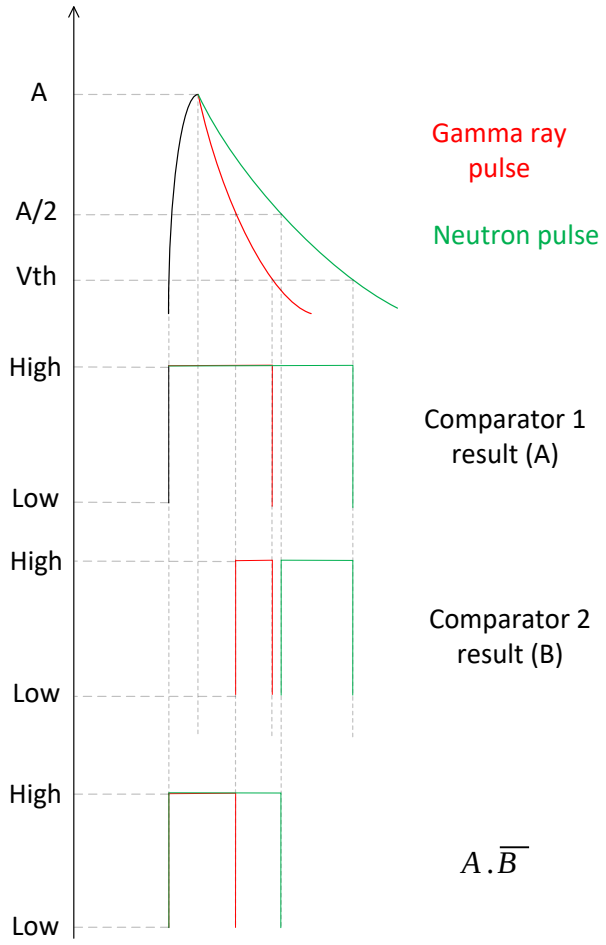


Figure 3.7: Timing signals for a gamma ray vs a neutron

We can see that the $A$ & $\bar{B}$ signal has different pulse widths for gamma and neutron where the pulse width for neutron is higher than the pulse width for gamma.

So, we need a pulse width detector to measure the pulse width and then convert this to binary information for pulse width binning.

For measuring the pulse width of $A.\bar{B}$ shown above, a basic time to digital converter (TDC) architecture is designed.

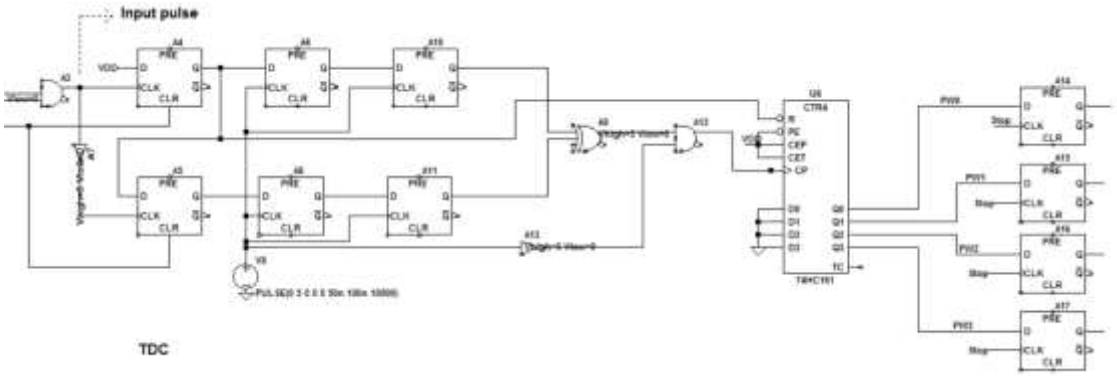


Figure 3.8: Schematic of the TDC

This TDC includes two D-flipflops (A4 and A5 in the schematic) one for detecting the rising edge and the other for the falling edge of the pulse. This rising edge and falling edge time are then sampled with respect to a clock signal. As these two signals are completely asynchronous to the clock, there is a problem of metastability.

Metastabilty is defined as the ability of a digital electronics system to persist for an unbounded time in an unstable equilibrium or metastable state [39]. In simpler words, when the D input to a flip flop comes from a source completely independent of the clock, it can move to any temporal location with respect to the clock. A problem arises when this D input changes at the same time or very near to the clock rising edge such that it doesn't meet the setup or hold time constraint of the D- flipflop. When this happens, the setup and/or hold node of the flip flop goes to an indeterminate state(X). If this state X propagate to the output, it can lead to a large number of devices turning on at the same time though they were not supposed to. This makes the current consumption very high which can potentially burn the whole circuit. Even if the output of the flip flop does not go to

indeterminate state, resolution of metastability can take a very long time of the clock period and thus lead to logic failures.

To prevent this metastability, two flip flop synchronizers are used both for the rising edge and falling edge pulses. Putting two flip-flops after each other gives the metastability state one complete clock cycle for the resolution and this is enough to meet the reliability demands in most cases. In some applications requiring very high speed data transmission coupled with extreme temperatures, there might be a need for more flip flops but nevertheless, in this application, speed is not that crucial as the pulse widths are about tenth of a microsecond. A more detailed analysis of metastability has been presented in [40] while [41] lists a variety of ways of dealing with metastability in addition to the two flip-flop synchronizers.

After dealing with metastability, these two signals are XORed together and used to mask the inverse of clock. Finally, this is used to drive the counter which generates the pulse width information by counting the number of clock cycles that occur in during the pulse. This circuit is very similar to the coarse measurement in [42]

The accuracy of this circuit is limited by the clock rate which has been discussed in results section. But again, the pulses are in 100s of μs while PLLs faster than 1GHz are readily available. That is why we do not need to add fine measurement in addition to the coarse. Should there arise a need for more accuracy later on, there are a variety of ways to boost the time resolution. One of these is the dual- slope interpolation method used in the above cited reference and in [43]. Then there are other digital methods which use tapped delay lines as the fine counter as in [44].

The pulse width has now been digitized. This information can now be loaded into a computer. The different pulse widths can be analyzed with a histogram which reports the distribution of gamma v/s neutrons as both of them have different numbers for the recorded pulse width information.

### 3.4 Event time binning

Now that we have designed the neutron-gamma discrimination circuitry, we also want to bin the events based on their arrival time at the instruments. It was established in Chapter-2 that we need this for the purpose of detecting water.

This is achieved in this system by measuring the time of each event and storing it along with the pulse width information. The design is as follows:

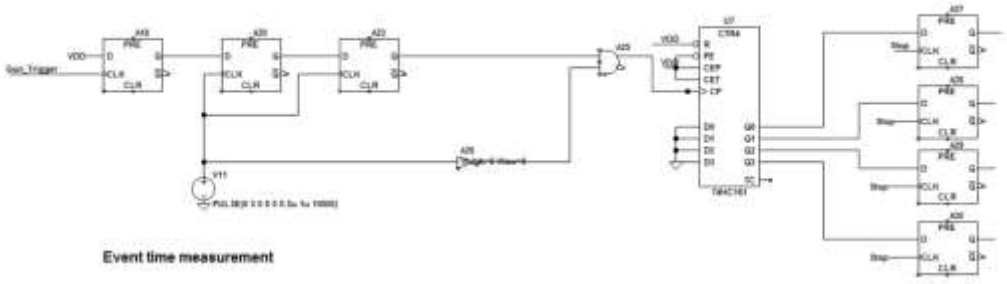


Figure 3.9: Schematic diagram of the circuit for event time measurement

This circuit takes two inputs Gun_Trigger and Stop. Gun_Trigger is a pulse which represents the turning ON of the neutron gun.

This Gun_Trigger is again sampled using two D-flipflops to prevent metastability. This is then used to drive a clock. This clock can be a lot slower than the clock signal for pulse width measurement which was 1MHz. Right now the model is using a clock of 100KHz but RMD has been using a window size of 65.536μs which means a clock period of 15.25 KHz. This slow clock will bin the events in a window size based on this clock period so a 10MHz clock will lead to a window size of 10μs while the 15.25KHZ clock bins it to a window size of 65.536 μs

The output bits of the counter are sampled at the falling edge of comparator 1 output which is denoted as the Stop net in the schematic. This Stop signal symbolizes the time instant when the current pulse finally decreases as compared to the threshold voltage.

### 3.5 Energy Measurement

Event energy measurement is one of the main functions of a spectrometer device. In this device, energy will be measured by using an integrator circuit with the amplified pulse being the input.

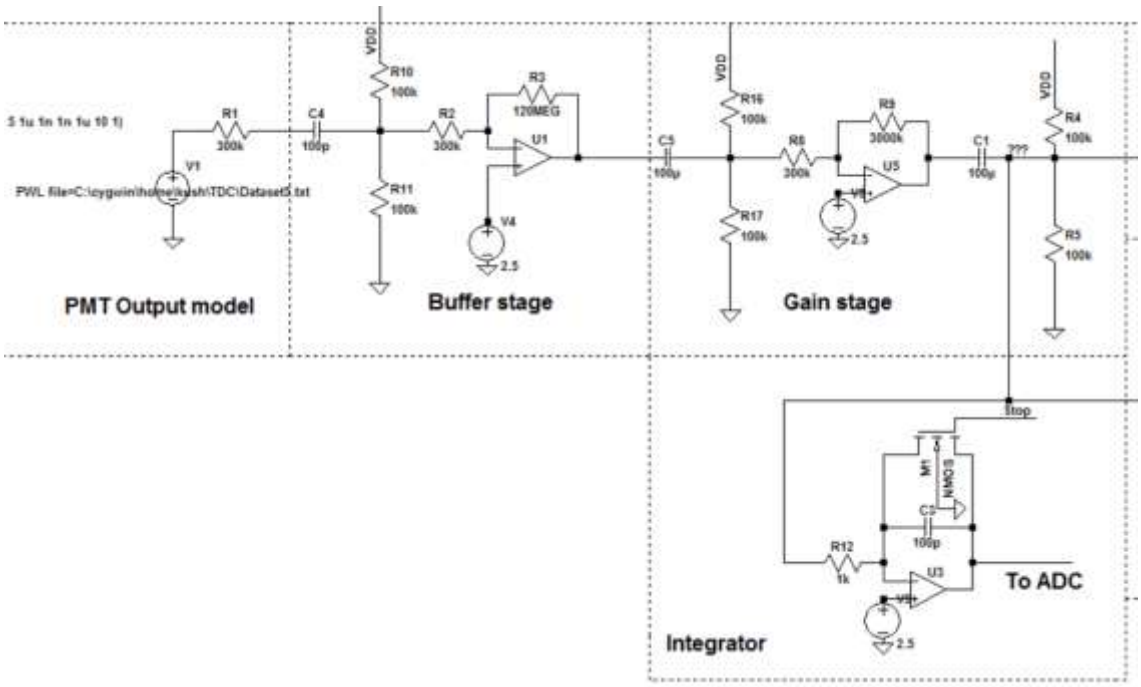


Figure 3.10: Schematic diagram with the integrator circuit

This design uses a basic OPAMP integrator with reset driven by the Stop signal because we do not want the integrator to get saturated at VDD and GND.

For a standard integrator:

We know that, $V_{out} = -\frac{1}{RC}\int_0^t V_{in}dt$

So, we can see that R and C value of the integrator are used to set the gain of the amplifier. This R and C are used to match the dynamic range of the amplified signal to the input dynamic range of the synchronous ADC this integrator is driving.

**ADC specifications:**

The observe pulse widths are of the order of 1μs. In the particular dataset considered with this design, there are at most 3 events in a window of 65.536μs. That means we need to sample two times in around a time of 10μs if we stay conservative. So, that means a sampling rate of 100Ksamples/ sec. The input dynamic range should be as large as possible for the maximum dynamic range of the input. So, 5V is a good number because there is definitely a 5V power supply on the CUBESAT as it is planned right now.

# CHAPTER 4

## Results

In this Chapter, the simulation results for the design are presented and compared with the results obtained by RMD on the same dataset. The dataset was collected by RMD using $Na^{22}AmBeCs^{137}$. AmBe is the neutron source and the other elements are source of gamma-rays. This data was collected at the ADC output of the system shown in Figure 4.1

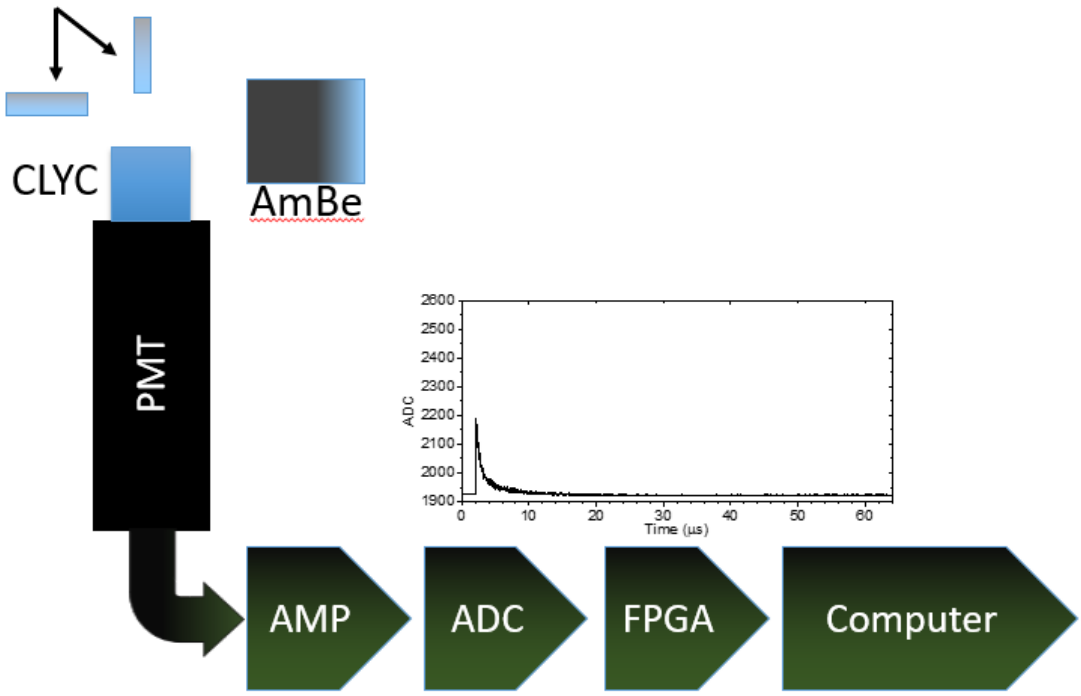


Figure 4.1: Overview of the system developed by RMD

This data is a good benchmark because of the already published results on it by RMD which provides both the discrimination of gamma and neutron as well as the event rate. But there

is one issue in using this data. The data comes from the output of an ADC according to their system while what we want is the PMT output. So, the data was backtracked to the PMT using data processing. The ADC used in this system is LTC-2158-14 and the AMP is LTC-6400-26. This is a 12-bit ADC with an input dynamic range of 1.32V. Thus, the 1.32V is converted to an output range of 0-4095. The AMP in the ADC driver configuration has a gain of 200V/V. So, the input from PMT goes through a gain of $\frac{200*4096}{1.32}$ before reaching to the ADC output. Thus, the data was divided by this number to get a good estimate of what the signal at the PMT output look like. This was done with a C program. This program also performed an added function of dividing the data into smaller segments because the data handling capacity of LTspice, the simulation software, is very limited.

The PMT data extraction was verified for correct functionality by using the scintillator and PMT on background data. The input impedance of the circuit was varied in order to minimize the effect of loading. It was found that 300KΩ is an optimal number for the input impedance. As the interface with PMT has been taken care of, the above cited dataset is a good test for the design.

### 4.1 Gamma-ray V/S neutron discrimination

As discussed in Chapter-3, in this design, the pulse width of the timing signal $A.\bar{B}$ is used to distinguish between gamma rays and neutrons. Thus, the pulse width of this signal is observed and plotted in the form of a histogram. The observed histogram is shown in figure 4.2.

As we can see gamma ray events can be easily seperated from the neutrons. The first peak corresponds to the gamma-ray events while the second peak corresponds to neutron events.

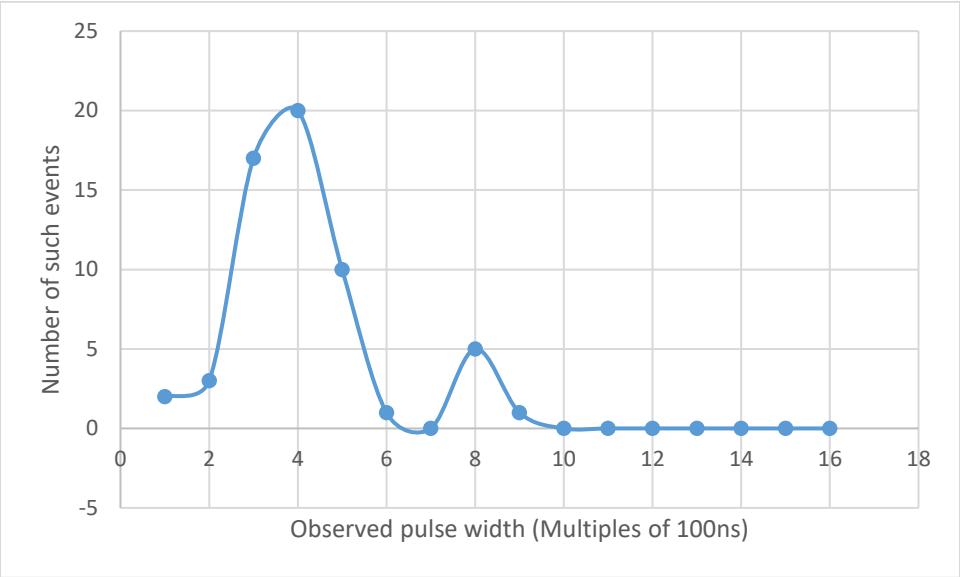


Figure 4.2: Histogram for the observed pulse widths of $A.\bar{B}$

These results are compared with the result obtained by RMD on the same dataset. Before presenting the result, there is a need to understand how their approach works.

In RMD's approach, the basis of detection is also the pulse shape discrimination. However there is a difference in how they use the shape of the pulse.

A generic gamma pulse is compared in Figure 4.3 with a neutron pulse. These duration of the pulses is divided into time windows and these pulses are integrated over these window of times. These times are fixed at 280ns, 680ns and 4000ns. The 4000ns window is used to measure the energy of the total pulse. The figure only shows the 280ns and 680ns windows because only these two are required for pulse shape discrimination.

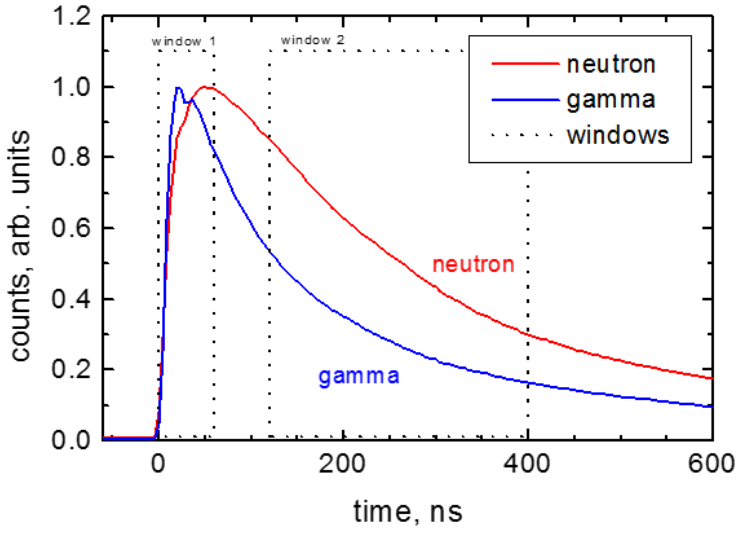


Figure 4.3: Gamma ray V/S a neutron shown in different windows

Notice that the integral of the signal for window 1 is almost equal for both gamma and neutron while integrals for window 2 is more for neutron as compared to gamma. So, if we use the integrals for window 1 and window 2 and divide integral 1 by integral 2, the quantity obtained will be higher for gamma-rays than neutrons. Here integral 1 acts as a normalization factor and we cannot just use integral 2 because the particles might have different energies which might result in no meaningful conclusion.

This ratio of integrals is called the PSD factor.

Thus, PSD = $\frac{\int_0^{280ns} p(t)dt}{\int_0^{680ns} p(t)dt}$

The result of this approach on the same dataset is presented in figure 4.4

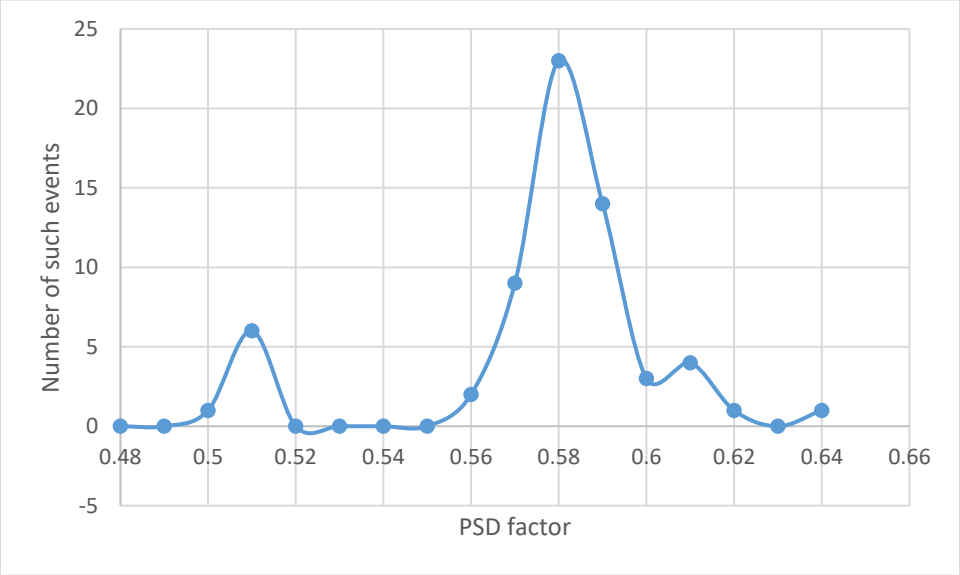


Figure 4.4: Histogram for the PSD factor obtaining by using the integral method

Note that the PSD factor is higher for gamma-ray than neutrons. Thus, the second peak corresponding to the gamma rays while first correspond to neutrons. We can clearly see a close correspondence between the two results.

For the design developed in this work, the peaks are 20 and 5 for gamma and neutron respectively while for neutron the peaks are 23 and 6 respectively.

Further, the total number of events detected by our approach is 59 as compared to 66 detected by RMD' s approach. The data was observed carefully to find the reason of this difference in recorded results and also to verify one to one correspondence in the neutron and gamma-ray events (meaning that the neutron events actually happen at the same time and not just a coincidence).

Thus, the dataset was divided into time windows of 327.68 μs and the number of events recorded was observed for both the approaches. This is presented in the Table 4.1 and 4.2

| Window | Number of gamma events | Number of neutron events |
|---|---|---|
| 1 | 6 | 0 |
| 2 | 7 | 0 |
| 3 | 5 | 0 |
| 4 | 6 | 0 |
| 5 | 4 | 2 |
| 6 | 5 | 0 |
| 7 | 4 | 1 |
| 8 | 6 | 1 |
| 9 | 3 | 2 |
| 10 | 7 | 0 |
| Total | 53 | 6 |

Table 4.1: Measurement dataset divided into windows for the pulse width method

As we can see, the number of events in each window is very close in both the methods though again there are a number of extra events in RMD's method. This was further investigated by checking the raw data for the events missing in our approach.

| Window | Number of gamma events | Number of neutron events |
|---|---|---|
| 1 | 7 | 0 |
| 2 | 9 | 0 |
| 3 | 5 | 0 |
| 4 | 6 | 0 |
| 5 | 5 | 2 |
| 6 | 6 | 1 |
| 7 | 4 | 1 |
| 8 | 6 | 1 |
| 9 | 4 | 2 |
| 10 | 7 | 0 |
| Total | 59 | 7 |

Table 4.2: Measurement dataset divided into windows for the integrator method

It was found that the difference is due to a lower threshold used in RMD's approach which leads to detection of pulses with lower energies. However, this lower threshold also has the added disadvantage of adding some false positives as was observed when going over the data pulse by pulse.

The data was also checked for one to one correspondence between the two results and it showed a complete match. Thus, it can be concluded that this new approach is also as effective as the tried and tested method used by RMD.

### 4.2 Measurement of energy

Energy measurement needs a lot of calibration regarding the R and C value of the integrator and the gain of amplifier stages. This is because of the inherent tradeoffs in this system. The bandwidth of the integrator or the speed with which a signal can be integrated is limited by the product of R and C. For maximum speed, you want R and C to be minimum. But C directly controls the charge holding capacity of the integrator. A smaller capacitor will be saturated by a short current pulse. Thus, there is an optimal level for this R and C. The amplifier gains need to be selected by considering the dynamic range of the system and the noise level. If the gain is too much, the output of the amplifier will get saturated to positive or negative rail for a short current pulse. On the other hand, if it is too low, some valid signals might be lost due to the input offset voltages and other non-linearity in the system. As such, it is harder to compare the energy with the energy observed by RMD. Thus, here the simulation results of the proposed design have been presented:

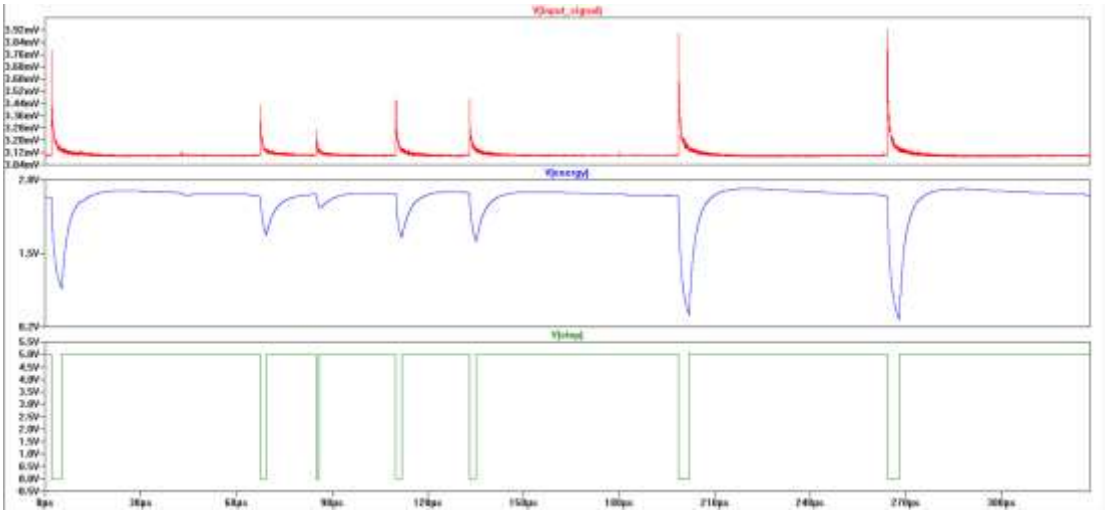

Figure 4.5: Simulation results for the energy of incident pulses for the proposed design

The input signal is integrated for the duration of the current pulse. This is represented in this figure by the duration for which the Stop signal is low. The energy keeps on accumulating until finally it is sampled at the rising edge of the Stop signal. At this point, most of the area under the signal has been integrated other than the time when the signal is already below threshold so it is an accurate estimate of the energy. Note that the energy signal goes on the negative side of the equilibrium point 2.5V. This is because this integrator is an inverting stage.

### 4.3 Timing errors

The pulse widths are measured in reference to a clock signal. As such, there is some timing error in the measurements. This can be calculated if we look at the timing diagram of a time to digital conversion (TDC) operation. In the TDC architecture used in this design, the input pulse is divided into two, unit step functions, one representing the rise and other the fall. These two signals are then clock synchronized. This is represented in Figure 4.5

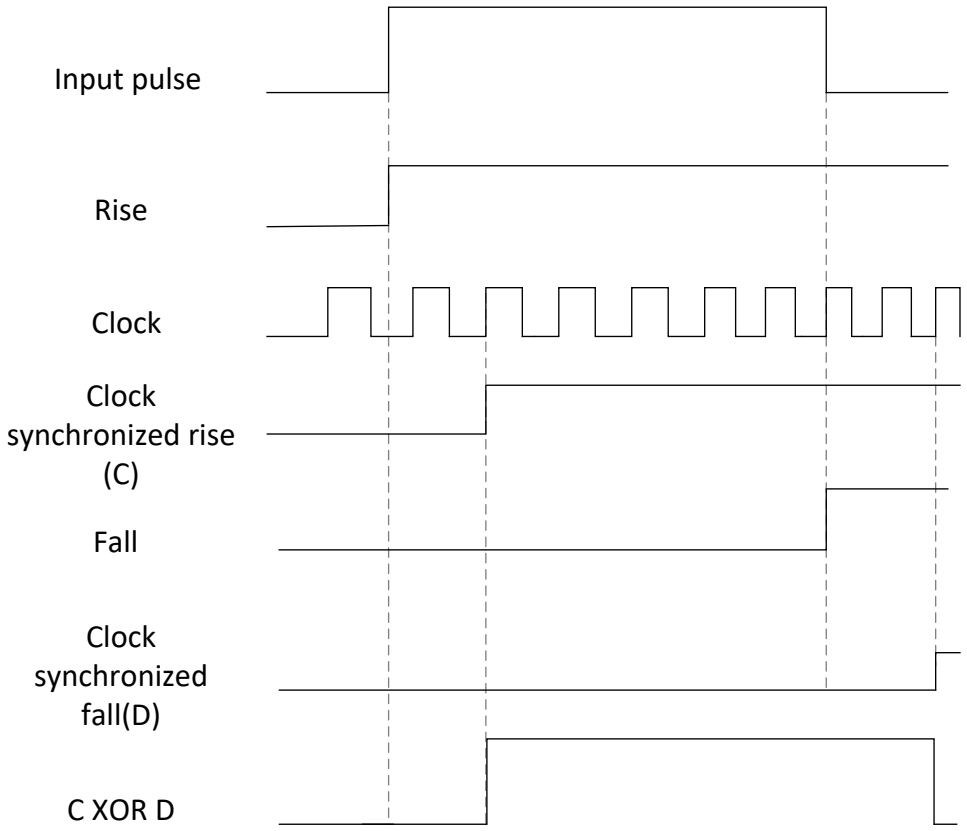


Figure 4.6: Timing diagram of the TDC outputs

In this scenario, the input pulse can change at any time with respect to the clock. If this input pulse comes just after a rising edge of clock, the effect of this clock will be only observed at the next clock rising edge. Thus, error in signal representing the rising edge information is equal to the period of the clock signal. Similarly, error in the signal representing falling edge information is also equal to the clock period. In this way, the total error in the output pulse width binary data is equal to 2*(time period of clock signal)

# CHAPTER 5

## Conclusion

An architecture for the readout electronics of a spectrometer device has been presented in this thesis. The spectrometer device uses novel scintillator material which can detect neutron and gamma-ray at the same time. So, the main challenge was the discrimination of gamma-rays from neutrons.

To deal with this, a novel method utilizing the time to reach half amplitude has been proposed. This has been supported with a mathematical analysis of the said design. An LTspice model for this design was simulated with data provided by a collaborating company which was collected using $Na^{22}AmBeCs^{137}$. The simulation was compared to a system developed by the said company for pulse shape discrimination in specific. The output matches to a large extent to the measurements made in previous attempts.

Next step is to expand on this design by building the system piece by piece on a board. Thus, the design will be migrated to a board design suite that offers schematic entry, simulation and layout as well.

Once the board is built, the system will be tested with other neutron and gamma sources. The current dataset includes the data from $Na^{22}AmBeCs^{137}$, some background data collected by placing the detector in ambient conditions and data collected from salt, KCl which is a neuron source. For preliminary testing the digital processing is done in a computer and an NI DAC is being used to transmit the analog information out of the amplifiers directly to the computer.

The ultimate target is to reduce the power consumed in the readout electronics and as such the design might be even migrated to an integrated circuit later on if it works out well on the board.

REFERENCES

[1] Pathways to Exploration: Rationales and Approaches for a U.S. Program of Human Space Exploration. Washington, D.C.: National Academies, 2014

[2] Nelson, Mark. "Mars water discoveries – implications for finding ancient and current life." Life Sciences in Space Research 7 (2015)

[3] Litvak, M. L., Mitrofanov I.G, Hardgrove C., et al. "Hydrogen and chlorine abundances in the Kimberley formation of Gale crater measured by the DAN instrument on board the Mars Science Laboratory Curiosity rover." Journal of Geophysical Research: Planets 121.5: pp. 836-45 (2016).

[4] Mitrofanov, Litvak, M. L., Sanin A.B, et al. "Water and chlorine content in the Martian soil along the first 1900 m of the Curiosity rover traverse as estimated by the DAN instrument." Journal of Geophysical Research: Planets, vol. 119, no. 7, pp. 1579-1596 (2014).

[5] Lucey, Paul G. "Radiative transfer modeling of the effect of mineralogy on some empirical methods for estimating iron concentration from multispectral imaging of the Moon." Journal of Geophysical Research 111.E8 (2006)

[6] Westlake, J. H., J. H. Waite, K. E. Mandt, N. Carrasco, J. M. Bell, B. A. Magee, and J.-E. Wahlund. "Titan's ionospheric composition and structure: Photochemical modeling of Cassini INMS data." Journal of Geophysical Research: Planets 117.E1 (2012)

[7] Bogue, Robert. "Mars curiosity: sensors on the red planet." Sensor Review 32.3, pp. 187-93 (2012)

[8] Siegbahn, Kai. Alpha- beta- and gamma-ray spectroscopy: vols 1-2. Amsterdam: North-Holland Pub. Co., 1965

[9] Curran, S.c. "Gamma-ray spectroscopy." Advances in Physics 2.8, pp. 411-49 (1953)

[10] Hertzog, R. "Elemental concentrations from neutron induced gamma ray spectroscopy." IEEE Transactions on Nuclear Science 35.1, pp. 827-32 (1988)

[11] Carpenter, J. M., and Chun-Keung Loong. Elements of slow-neutron scattering: basics, techniques, and applications. Cambridge: Cambridge U Press, 2015

[12] Mitchell, P. C. H. Vibrational spectroscopy with neutrons: with applications in chemistry, biology, materials science and catalysis. Singapore: World Scientific, 2005

[13] Ramirez-Cuesta, A.j., M.o. Jones, and W.i.f. David. "Neutron scattering and hydrogen storage." Materials Today 12.11, pp. 54-61(2009)

[14] Nikl, Martin, and Akira Yoshikawa. "Recent R&D Trends in Inorganic Single-Crystal Scintillator Materials for Radiation Detection." Advanced Optical Materials 3.4, pp 463-81 (2015)

[15] Krane, Kenneth S. Modern physics. Hoboken, NJ: Wiley, pp. 75-95 (2012)

[16] Klassen, Stephen. "The Photoelectric Effect: Reconstructing the Story for the Physics Classroom." Science & Education 20.7-8, pp. 719-31 (2009)

[17] Eisenberger, P., and P. M. Platzman. "Compton Scattering of X Rays from Bound Electrons." Physical Review A 2.2, pp. 415-23 (1970)

[18] Pratt, R.h., L.a. Lajohn, V. Florescu, T. Surić, B.k. Chatterjee, and S.c. Roy. "Compton scattering revisited." Radiation Physics and Chemistry 79.2, pp. 124-31 (2010)

[19] Hubbell, J.h. "Electron–positron pair production by photons: A historical overview." Radiation Physics and Chemistry 75.6, pp. 614-23 (2006)

[20] Bulanov, S. S., N. B. Narozhny, V. D. Mur, and V. S. Popov. "Electron-positron pair production by electromagnetic pulses." Journal of Experimental and Theoretical Physics 102.1, pp. 9-23 (2006)

[21] Selim, F.a., D.p. Wells, J.f. Harmon, J. Kwofie, G. Erikson, and T. Roney. "New positron annihilation spectroscopy techniques for thick materials." Radiation Physics and Chemistry 68.3-4, pp. 427-30 (2003)

[22] Glodo, J., (2008) Scintillation Properties of 1 Inch Cs2LiYCl6:Ce Crystals. IEEE Transactions on Nuclear Science, Vol 55, No 3.

[23] Brooks, F. D., Klein H., “Neutron spectrometry-historical review and present status”, Nucl. Instruments and Methods in Physics Research A 476 (2002)

[24] Stonehill, Laura C. "A New Scintillator for Neutron and Gamma Detection: Cs2LiYCl6:Ce3 (CLYC) Overview and Selected Applications." (2012)

[25] Machrafi, R., N. Khan, and A. Miller. "Response functions of Cs2LiYCl6: Ce scintillator to neutron and gamma radiation." Radiation Measurements 70 (2014)

[26] Smith, M.b., T. Achtzehn, H.r. Andrews, E.t.h. Clifford, P. Forget, J. Glodo, R. Hawrami, H. Ing, P. O’Dougherty, K.s. Shah, U. Shirwadkar, L. Soundara-Pandian, and J. Tower. "Fast neutron measurements using Cs2LiYCl6:Ce (CLYC) scintillator." Nuclear Instruments and Methods in Physics Research Section A: Accelerators, Spectrometers, Detectors and Associated Equipment 784 (2015)

[27] N. D'Olympia, P. Chowdhury, C. J. Guess, et al., “Optimizing Cs2LiYCl6 for fast neutron spectroscopy,” Nuclear Instruments and Methods in Physics Research Section A, vol. 694, pp. 140-146, 2012

[28] N. D'Olympia, P. Chowdhury, C. J. Lister, et al., “Pulse-shape analysis of CLYC for thermal neutrons, fast neutrons, and gamma-rays,” Nuclear Instruments and Methods in Physics Research Section A, vol. 714, pp. 121-127, 2013

[29] B. S. Budden, L. C. Stonehill, J. R. Terry, et al., “Characterization and Investigation of the Thermal Dependence of Cs2LiYCl6:Ce3+ (CLYC) Waveforms,” Nuclear Science, IEEE Transactions on, vol. 60, pp. 946-951, 2013

[30] J. Glodo, R. Hawrami, E. Van Loef, et al., “Pulse Shape Discrimination With Selected Elpasolite Crystals,” Nuclear Science, IEEE Transactions on, vol. 59, pp. 2328-2333, 2012.

[31] Brittany Morgan, “Neutron-Gamma Discrimination in Elpasolite Scintillator Detector”, University of Nevada, Masters thesis. Proquest, http://search.proquest.com.ezproxy1.lib.asu.edu/docview/1812321937?pq-origsite=summon

[32] "Photomultiplier." Wikipedia: The Free Encyclopedia. Wikimedia Foundation, Inc. 28 January 2017. Web. 15 Feb. 2017.

[33] Hamamatsu Photomultiplier Tube R11265U series, Feb 2016. https://www.hamamatsu.com/resources/pdf/etd/R11265U_H11934_TPMH1336E.pdf

[34] Cadamuro, L., M. Calvi, L. Cassina, et al. "Characterization of the Hamamatsu R11265-103-M64 multi-anode photomultiplier tube." Journal of Instrumentation 9.06 (2014)

[35] Hakamata T., Kume H., Okano K., et al. Photomultiplier Tube Basics and Applications: Third edition: Hamamatsu Photonics K.K. (2007) https://www.hamamatsu.com/resources/pdf/etd/PMT_handbook_v3aE.pdf

[36] Texas Instruments Wideband Operational Amplifier THS4509, July 2016. http://www.ti.com/product/ths4509/datasheet

[37] Maxim Integrated Application Note 3616, Adding Extra Hysteresis to Comparators, Sep 19, 2005. https://www.maximintegrated.com/en/app-notes/index.mvp/id/3616

[38] EEV blog #490, Designing and measuring basic and precision opamp peak detector circuits, Jun 29, 2013. https://www.eevblog.com/2013/06/29/eevblog-490-peak-detector-circuit/

[39] "Metastability in electronics" Wikipedia: The Free Encyclopedia. Wikimedia Foundation, Inc. 20 April 2017. Web. 20 April 2017.

[40] Kalisz, J., and Z. Jachna. "Metastability tests of flip–flops in programmable digital circuits." Microelectronics Journal 37.2, pp. 174-80. (2006)

[41] Semiat, Y., and R. Ginosar. "Timing measurements of synchronization circuits." Ninth International Symposium on Asynchronous Circuits and Systems, 2003

[42] T. Copani, B. Vermeire, A. Jain, H. Karaki, K. Chandrashekar, S. Goswami, J. Kitchen, H. H. Chung, I. Deligoz, B. Bakkaloglu, H. Barnaby, and S. Kiaei, “A fully integrated pulsed-LASER time-of-flight measurement system with 12ps single-shot precision,” 2008 IEEE Custom Integrated Circuits Conference, 2008

[43] Raisanen-Ruotsalainen, E., T. Rahkonen, and J. Kostamovaara. "An integrated time-to-digital converter with 30-ps single-shot precision." IEEE Journal of Solid-State Circuits 35.10, pp. 1507-510 (2000)

[44] R. Szplet, J. Kalisz, and R. Szymanowski, “Interpolating time counter with 100 ps resolution on a single FPGA device,” IEEE Trans. Instrum. Meas. IEEE Transactions on Instrumentation and Measurement, vol. 49, no. 4, pp. 879–883, Aug. 2000.